J. Fluid Mech. (1971), *vol.* 50, *part* 1, *pp.* 49–78
Printed in Great Britain

The near field within the potential cone of subsonic cold jets

By N. W. M. KO† AND P. O. A. L. DAVIES
Institute of Sound and Vibration Research, University of Southampton

(Received 18 March 1971)

This investigation describes a detailed study of the near pressure field within the potential cone of a subsonic circular turbulent jet.

The components of the near pressure field in the potential cone in which the potential flow condition exists within the first four and a half diameter downstream appear to be moving with a phase velocity equal to the local speed of sound. The direction of propagation is roughly normal to the shear layer surrounding the cone. Some components of the hot-wire signal can be associated with the jet structure as a simple complex source, while others are related to the local characteristics of turbulence. Differences in the characteristics of the pressure field within the potential cone exist between the vortex generated noise at very low jet velocity and the eddy generated noise at higher velocity.

The power spectra obtained in the potential cone show the peak which is due to the pressure fluctuations and the flat portion due to the turbulence. The frequencies of the dominant components, in terms of the Strouhal number, are functions of both the axial and radial positions.

Microphone measurements were made in the near field outside for detailed comparison with the potential cone results.

1. Introduction

The far field of the jet is not a good region in which to try to further the understanding of the noise generation by turbulence. At such a long distance away from the noise producing region, the jet behaves like a single source. Thus, a vast amount of detail about the individual sources, intermixing among themselves and interacting with the local turbulence, would be lost by this single source behaviour in the far field.

The near field outside the jet offers a better opportunity for study of the behaviour of the different sources existing in the shear region. The pressure measurements of Franklin & Foxwell (1958) and Mollo-Christensen (1963) and others show the domination of the nearest sources and this domination is more severe as the jet boundary is approached. However, the pressure fluctuations of the near field are completely free of the influence of the turbulence and the

† Present address: Department of Mechanical Engineering, University of Hong Kong, Hong Kong.

complication arising from the intermixing between the density variation due to the pressure field and local turbulent fluctuations cannot be investigated.

With this limitation of the near field in mind, the best region for the investigation of the pressure fluctuations will be the shear region itself. However, the difficulty in separating the pressure fluctuations from the strong local turbulence has to be realized. The only successful attempts have been made by Davies, Ko & Bose (1967) and Bose (1968) by using Fourier transforms on the measurements of the space correlograms from a very stable correlator. Preliminary results show the presence of pressure fluctuations even in the strong turbulent field. Even so, the separation of the individual effect of turbulence is still not available.

A region which is almost as good, is the near field inside the potential cone. It has the advantage of low turbulence which offers easier separation between the pressure and turbulence fields. But no pressure measurement is available to shed any light on this field inside, not mentioning the complication due to turbulence and individual sources. Besides the complete absence of pressure measurements, the measurements of the statistical properties of the flow within the potential cone are very crude and scarce. For this lack of data, the usual, but not necessarily right, assumption of potential flow inside the jet has to be blamed.

The purpose of the present investigation was to obtain information about the pressure field inside the potential cone. The method for this investigation is based on the well-established fact that the hot wire measures the instantaneous local mass flux (Davies & Ko 1965 and Davies, Ko & Bose 1967). This means that the fluctuating hot-wire signal consists of two components, one from density and the other from velocity fluctuation. At moderate or low Mach numbers the density fluctuations due to the pressure field may not be small, as is usually assumed, compared with the local velocity fluctuations, especially when the latter are very small as in the potential cone. These density fluctuations, as will be shown later, are really the dominating term of the hot-wire signals obtained in the cone, while the local velocity fluctuations only contribute a smaller part.

Comparison with the near field outside will be made. Unfortunately, the available measurements from other workers are not detailed enough for direct comparison. Thus, detailed microphone measurements have to be made and are presented.

2. Experimental apparatus

For the present investigation both 2·5 cm and 5·0 cm diameter nozzles were used. The area contraction ratio of the nozzles was 9:1. Both nozzles were supplied with dry oil-free high pressure air from three large air reservoirs. The nozzles have a Burgess-type silencer as the settling chamber and the noise from the control gate valves was mostly absorbed before it arrived at the nozzle exit.

Constant-temperature hot-wire anemometers with linearizers were used during the investigation. The wire, of length 2 mm and diameter 5×10^{-6} m, has a working resistance of 15 ohms. The details of the anemometers, linearizers and manufacturing of hot wires were discussed by Davies & Fisher (1964) and Ko

(1969). The linearity of the combined unit of anemometer and linearizer was achieved from 12 m/sec to 110 m/sec. Slight deviation was observed below and above this range.

Interference between two hot wires was found due to the hot and cold wakes of the wire (Ko & Davies 1971). This effect is very severe when the local turbulence fluctuations are small in comparison with the ones of the wake, such as in the potential cone of the jet. Thus for two wires, including cross-wires, any measurements without proper consideration of the interference effect as found by Ko & Davies (1971) could be misleading.

The analogue correlator used has been described by Allcock, Tanner & McLachlan (1962). A sampling correlator was built in Southampton which gave a flat frequency response from 20 Hz to 40 kHz (Ko 1969). The frequency analyzer used was a Brüel & Kjaer frequency analyzer, Type 2107 with a 6% constant percentage bandwidth, together with a Brüel & Kjaer level recorder, Type 2305.

The microphone used for outside pressure measurements was a Brüel & Kjaer quarter-inch condenser microphone, Type 4135. It was used without the protecting grid and gave a flat frequency response from 50 Hz up to 20 kHz for normal incidence and to 5 kHz for 90° grazing incidence.

3. Results

The domain of investigation will mostly be confined to the potential cone, which is $\eta = (y - \frac{1}{2}D)/x \leqslant 0, x/D \leqslant 5$ and a Mach number less than 0·45 (figure 1). For microphone measurements outside the jet, the region covered is within the radial distance of one diameter away from the jet boundary $\eta \geqslant 0{\cdot}17$ ($\theta = 10°$).

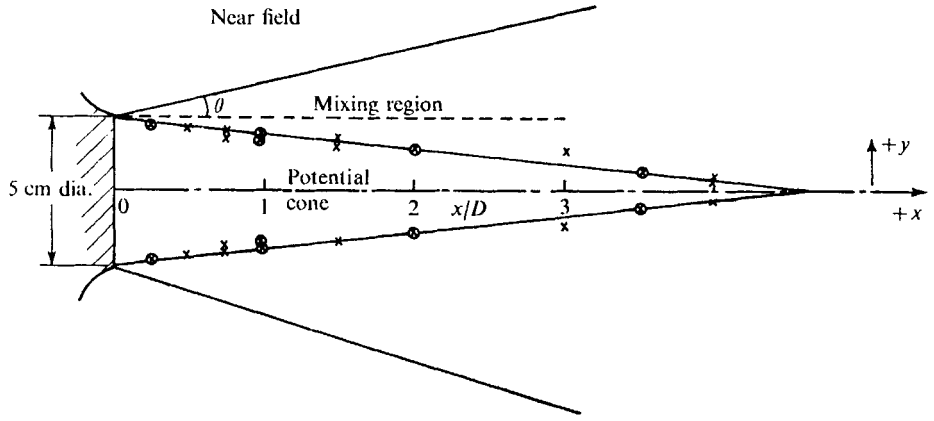

FIGURE 1. Profile of the potential cone of 5 cm diameter jet. ○, pitot; ×, hot wire.

3.1. *Mean velocity*

Similarity of the mean velocity ratio profile, $\overline{U}/\overline{U}_0$, with the non-dimensional radial distance, η, is true only between the axial distance $x/D = 1{\cdot}0$ to 4, as shown in figure 2. The nearer to the nozzle exit, the more deviation of the velocity

ratio profile from the similarity curve. From the profile, the potential cone boundary more or less terminates at the non-dimensional radial distance of $\eta = -0{\cdot}105$ (figure 1).

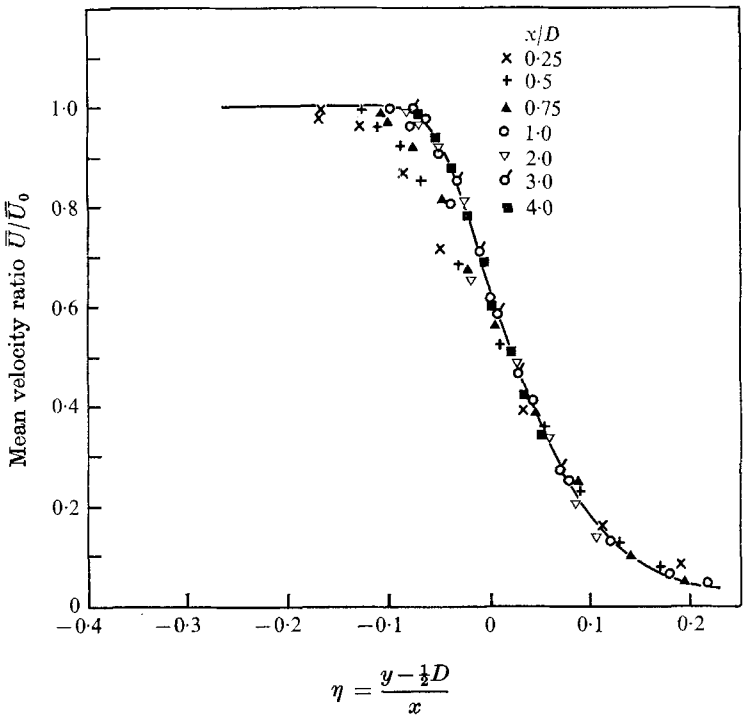

FIGURE 2. Non-dimensional plot of mean velocity ratio.
Jet diameter = 5 cm, $M_0 = 0{\cdot}218$.

3.2. *Turbulence intensity within the potential cone*

Although a lot of work has been done on turbulence intensity in the mixing region of a jet, such as the results of Laurence (1956), Davies, Fisher & Barratt (1963) and others, the turbulence level inside the potential cone has not been seriously considered, especially with the effect of the exit velocity.

The axial and radial distribution of the turbulence intensity level within the potential cone is shown in figure 3. For the radial position of $y/D \leqslant 0{\cdot}2$ the turbulence level for any axial position $x/D \leqslant 4{\cdot}5$ is fairly small, about 3% of the mean exit velocity. The effect of the turbulence in the mixing region is felt more as the axial and radial positions increase.

The variation of the turbulence intensity level, $(\overline{u^2})^{\frac{1}{2}}/\bar{U}_0$, with the jet exit Mach number is shown in figure 4 (*a*). The results are for the 2·5 cm diameter jet. Similar results were obtained from the 5·0 cm diameter jet, but are not shown here. For the axial position $x/D \leqslant 0{\cdot}25$, figure 4 (*a*) shows no variation in intensity with the exit Mach number. At the axial position of $x/D = 0{\cdot}5$ there is a gradual increase at low exit Mach number. A rapid increase occurs at $x/D = 2{\cdot}5$ and 3·5.

At low exit Mach number, the results from figure 4(*a*) show a sudden increase in the intensity level obtained by the hot wire. This increase is more obvious at larger axial distances. This transition from low to high velocity is very pronounced. Besides the high intensity level below a Mach number of 0·06, two smaller 'rises' are present at Mach numbers of roughly 0·08 and 0·2. These can more easily be seen in the plot of the absolute r.m.s. fluctuating velocity, $(\overline{u^2})^{\frac{1}{2}}$, as shown in figure 4(*b*). Here the peaks of the intensity definitely stand out from the increasing background at Mach numbers of 0·04, 0·10 and 0·2. The one at Mach number 0·08 shown in figure 4(*a*) is not so obvious. Although the 5 cm diameter jet results are not shown in this paper, the exact agreement with figure 4(*a*) and (*b*) in the Mach numbers at which the 'rises' occur rules out any singularity of result due to the reading of only one jet.

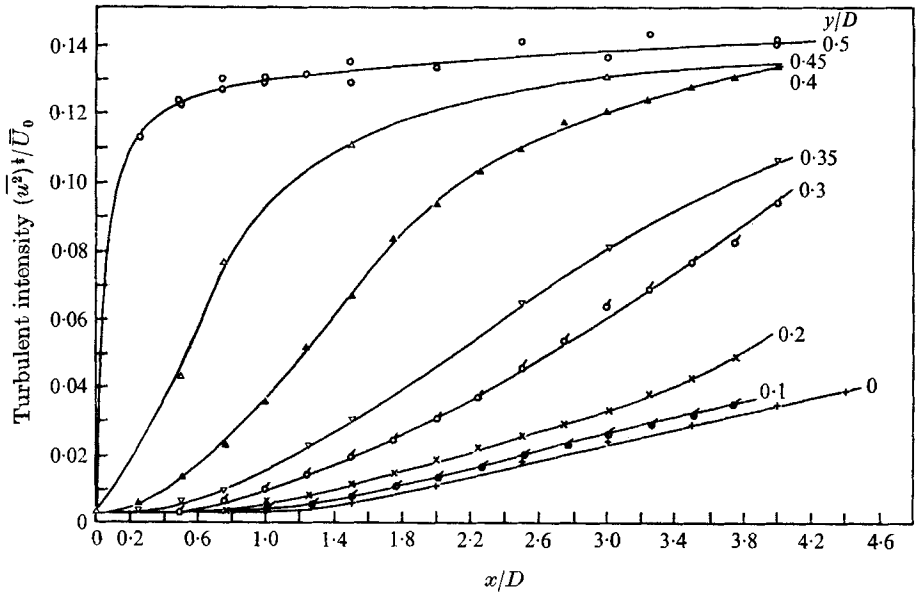

FIGURE 3. Turbulent intensity against axial distance. 5 cm diameter jet, $M_0 = 0{\cdot}22$.

It has been shown by the gas injection schlieren photographs of Bradshaw, Ferriss & Johnson (1964) that vortex rings exist at the Mach number of roughly 0·04 within the first diameter downstream. Thus, the Mach number at which the vortex rings exist falls nicely on the peak of the fluctuating r.m.s. velocity graph, figure 4(*b*).

Although the agreement shown is good, allowances for a large percentage of experimental error have to be made because of the small values of the mean and r.m.s. voltages. It was also observed that fairly large fluctuations of the meter needle occurred at the low exit velocity. This suggests that fairly large fluctuations either of density or velocity, or both, were sensed by the hot wire which was situated inside the potential cone.

Oscilloscope photographs of the signal received by the hot wires are shown in figure 5(*a*) to (*c*) at the axial position $x/D = 0{\cdot}5$ and radial positions of

$y/D = 0$, 0·5 and 0·6. The jet exit Mach number was about 0·01. From figure 5(*b*) fairly repeatable signals are obtained by the hot wire in the mixing region. At the axis, $y/D = 0$ (figure 5(*a*)), there are sudden increases in amplitude which appear in the centre of the photograph, and then are maintained at lower amplitude until the next burst.

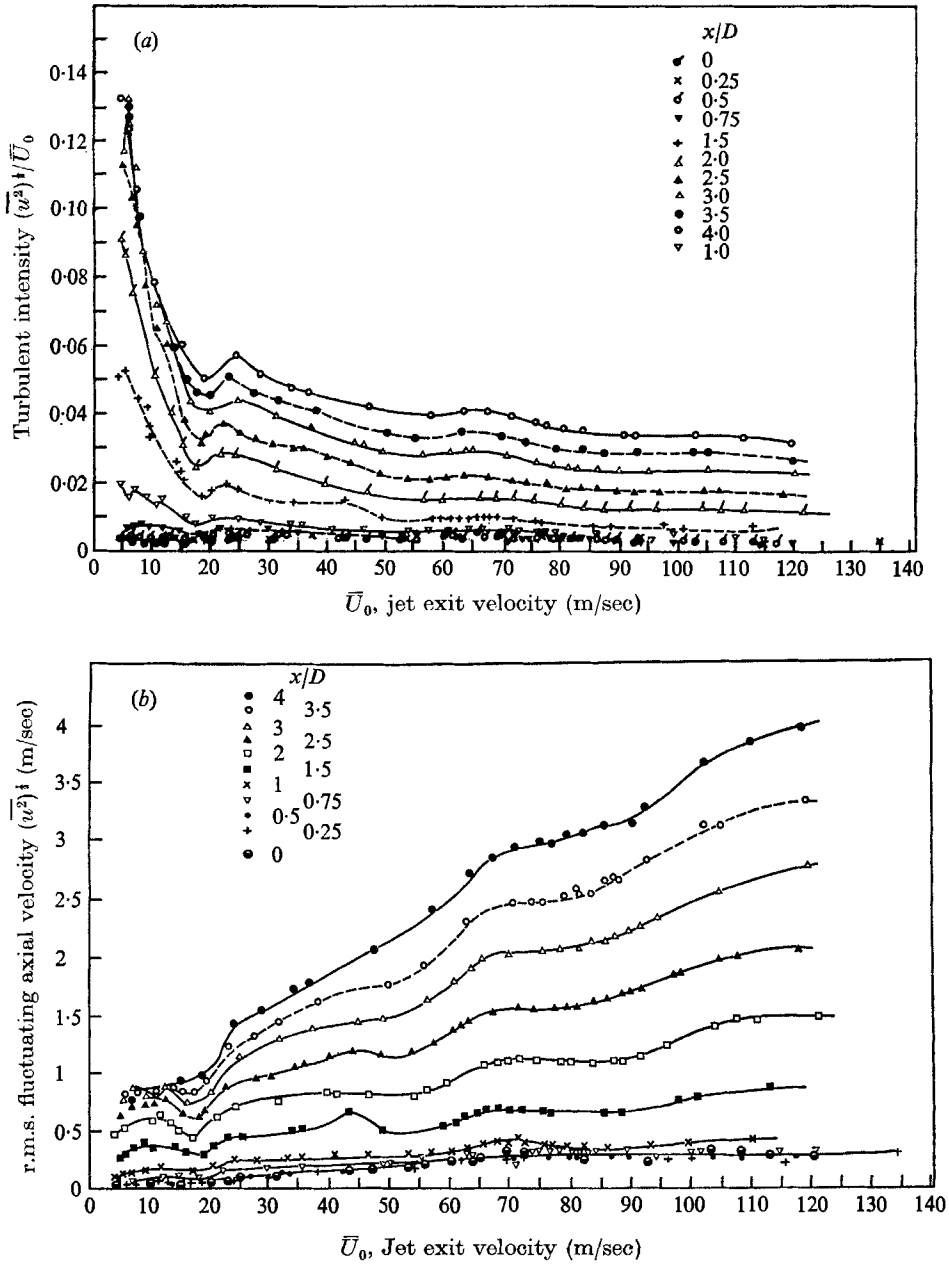

FIGURE 4. (*a*) Turbulent intensity and (*b*) r.m.s. fluctuating axial velocity against jet exit velocity for different axial positions along the axis. 2·5 cm jet diameter, $y/D = 0$.

Another phenomenon observed during experiment was that below a Mach number of 0·06 a discrete tone could be heard above the valve noise and the noise produced by the jet. This discrete tone persisted until the Mach number of 0·06 was reached before it was drowned by the increasing jet noise.

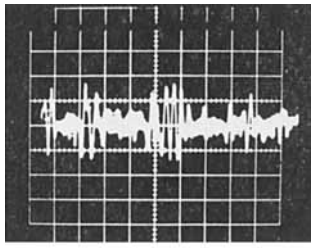

(*a*) $x/D = 0{\cdot}5, y/D = 0$ (in the potential cone)
Vertical scale 50 mV/cm
Horizontal scale 50 msec/cm
Jet exit velocity $\bar{U}_0 = 5$ m/sec
(mean voltage 1 V)

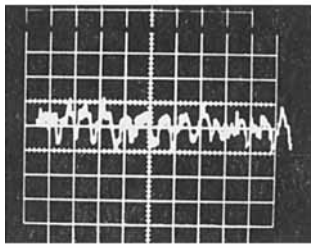

(*b*) $x/D = 0{\cdot}5$, $y/D = 0{\cdot}5$ (in the mixing region)
Vertical scale 0·5 V/cm
Horizontal scale 20 msec/cm
Jet exit velocity $\bar{U}_0 = 5$ m/sec
(mean voltage 0·7 V)

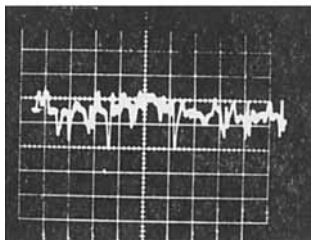

(*c*) $x/D = 0{\cdot}5$, $y/D = 0{\cdot}6$ (in the mixing region)
Vertical scale 0·2 V/cm
Horizontal scale 20 msec/cm
Jet exit velocity $\bar{U}_0 = 5$ m/sec
(mean voltage 0·2 V)

FIGURE 5

The above-mentioned evidence suggested that the high turbulence intensity observed inside the cone at the Mach number of 0·06 is due to the hydrodynamic pressure field associated with the vortices formed at the jet exit. Thus, the hot wire on the axis of the jet not only senses the local turbulence fluctuating velocity but also the dominant hydrodynamic pressure field associated with the vortices. This would then explain the sudden burst of signals shown in figure 5(*a*), representing the passing by of the vortices and the pressure field associated with them.

Below a Mach number of 0·06 the independence of the fluctuating r.m.s. velocity with respect to the axial position within the first half diameter suggests directionality of the pressure field into the potential cone. This can be seen from the difference in the axial distance between the schlieren photographs of

Bradshaw *et al.* (1964), which show that the visible vortices are present within the first half diameter, and figure 4(*b*) where the peaks start their appearance from $x/D = 0{\cdot}75$ onwards.

By establishing that the increase in the r.m.s. fluctuating velocity below the Mach number of 0·06 is due to the presence of the hydrodynamic pressure field associated with the vortices propagated into the potential cone, the same reasoning can be applied to the other two peaks at the Mach numbers 0·10 and 0·20. The sudden increase may be due to the extra increase of the pressure field from the mixing region, and the reason for it is not yet known. However, it seems that the pressure field associated with the vortices in the low velocity case and the eddies in the medium and high velocity cases, does not increase smoothly, but in small gradual 'steps'. This argument is not at all unreasonable because the readjustment or rearrangement among the 'eddies' themselves has to be made beyond a certain velocity range. This is clearly shown by the appearance of the vortices, then their disappearance, and the pressure field associated with them. In the medium and high velocity range, because of the random nature of different eddies which may be at equal and opposite phase, summation and cancellation of the pressure fields emitted may occur. The amount of summation and cancellation may be different with respect to the exit velocity and this may result in the 'step' in the intensity curve as obtained above.

3.3. *Radial cross-correlation coefficient in the potential cone*

The radial cross-correlation coefficient between two radially separated wires is defined as $R_{y\tau} = \overline{u(y)\,u(y+\Delta y,\tau)}/\hat{u}(y)\,\hat{u}(y+\Delta y,\tau)$. The results are shown in figure 6. Since the fixed wire was situated at the axis, $y/D = 0$, and the other wire was moving in the y direction and was delayed, a field convecting from the moving wire to the fixed wire will give a shift of the peak of the cross-correlation curve in the direction of positive time delay.

The extremely good correlation even at a separation of $y/D = 0{\cdot}3$ as shown on figure 6 indicates that the same field is mainly responsible for the correlation results within the potential cone. This good correlation at such a separation rules out the presence of eddies inside the potential cone because measurements in the mixing region show that the maximum radial cross-correlation was never found greater than 0·2 even for a radial separation of $\Delta y/D = \pm 0{\cdot}1$.

3.4. *Radial convection velocity in the potential cone*

The most important result from figure 6 is the tendency for a slight shift of the peak coefficient to the positive direction of the time delay, τ. With increasing radial separation, the positive shift increases. This positive shift indicates that the direction of propagation of the highly correlated field is from the mixing region into the potential cone. By defining the velocity of convection or propagation in the radial direction, $\overline{V}_c$, as the ratio of the the radial wire separation to the corresponding time delay, τ, at which the coefficient attains its maximum, the radial convection velocity can be obtained and is shown in table 1. The negative sign means the convection velocity is in the opposite direction to $+y$, that is, propagating from the mixing region into the potential cone.

From table 1 the radial convection velocity is of the order of the speed of sound over a certain radial distance and then abruptly attains a value of about 150 m/sec or less. The region in which the radial convection velocity attains the speed of sound is plotted in figure 7. The direction of the convection velocity is from the mixing region into the potential cone.

The above evidence strongly suggests that there is a pressure field propagating into the potential cone. Because the distance of the potential cone from the

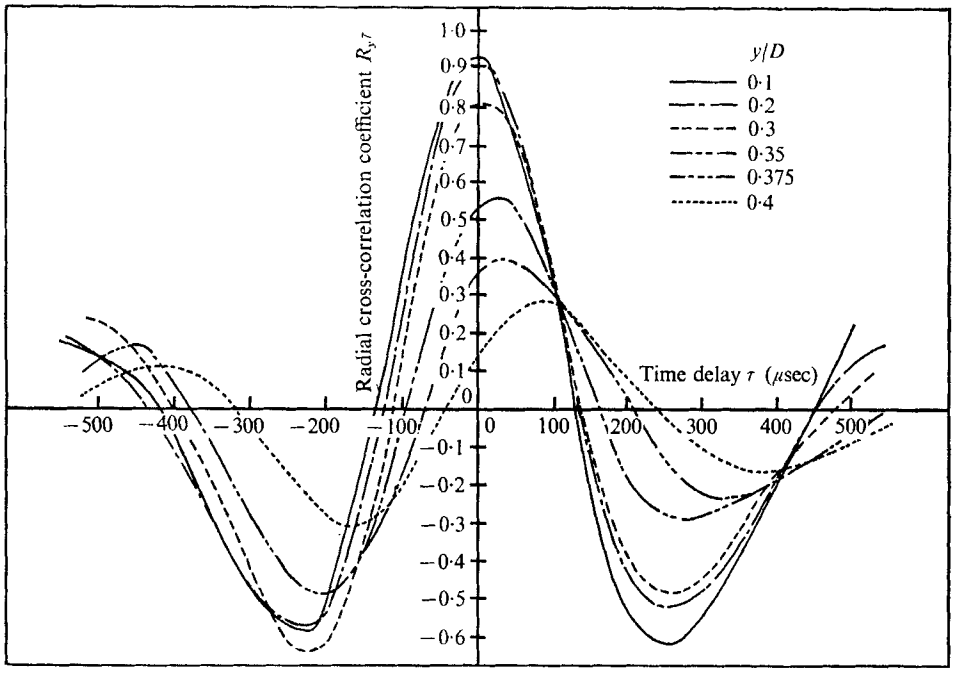

FIGURE 6. Radial distribution of cross-correlation coefficient. 2·5 cm diameter jet, $x/D = 1{\cdot}5$, $M_0 = 0{\cdot}22$. Fixed wire at $y/D = 0$ and moving wire delayed with respect to fixed wire.

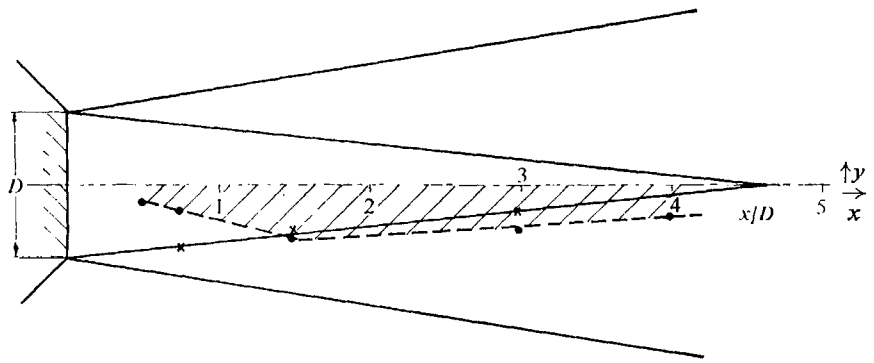

FIGURE 7. Profile of the potential cone of the jet. A cross denotes the position of the highest radial frequency or Strouhal number and the shaded area is the area under which the convection velocity in the y direction attains the order of the velocity of sound.

(*a*) Jet diameter 5 cm, $M_0 = 0{\cdot}218$

x/D	y/D	0·05	0·1	0·15	0·2	0·25	0·3	0·35	0·4	0·45	0·5	0·6
0·5	τ	−7·5	−15	−50	−200	−250	−100	−50	−150	−200	?	?
				−20			−150					
	$\bar{V}_c$	−338	−338	−153	−51	−51	−153	−354	−136	−114	?	?
				−387			−99					
0·75	τ	?	−15	−20	−100	−100	−100	−85	−100	−200	−300	?
	$\bar{V}_c$	?	−338	−378	−102	−127	−153	−210	−204	−114	−69	?
1·5	τ	−10	−15	−20	−25	−30	−35	−50	−135	−225	−350	+350
			−10		−20		−40		−150	−250		
	$\bar{V}_c$	−253	−338	−381	−410	−420	−426	−354	−151	−102	−73	−88
			−506		−506		−378		−136	−92		
3·0	τ	−10	−15	−20	−20	−40	−50	−125	−170	−200	+200	+400
				−15	−15	−30	−70					
	$\bar{V}_c$	−253	−338	−378	−506	−317	−305	−142	−119	−114	+127	+76
				−506	−424	−424	−216					
4·0	τ	−15	−15	−30	−35	−100	−150	−100	—	—	—	—
								−120				
	$\bar{V}_c$	−506	−338	−254	−291	−127	−102	−153	—	—	—	—
								−148				

(*b*) Jet diameter 2·5 cm, $M_0 = 0{\cdot}22$

x/D	y/D	0·1	0·2	0·3	0·35	0·375	0·4
1·5	τ	—	—	—	—	—	—
	$\bar{V}_c$	−305	−510	−445	−354	−317	−131
3·0	τ	—	—	—	—	—	—
	$\bar{V}_c$	−305	−405	−152	−101	—	—

TABLE 1. Radial convection velocity at different axial positions. Fixed wire at $y/D = 0$, τ = time delay (μsec), $\bar{V}_c$ = radial mean convection velocity (m/sec)

mixing region is so small, much less than a wavelength of the low and medium frequency sound, the pressure field inside the potential cone can be considered as a near field.

The shaded region in figure 7 definitely occupies not only the full volume of the potential cone ($x/D \geqslant 1{\cdot}5$), but also a small part of the mixing region. Outside this volume, the convection velocity obtained is only about 150 m/sec. Moreover, this boundary marks the positions where the turbulence intensity increases very rapidly with radial distance.

The low convection velocity observed within the first one and a half diameters may be due to the directivity of the pressure field propagating into it. It may also be due to the large refraction which occurs within the smaller mixing region. However, there is not sufficient evidence to decide which is correct.

Although the inaccuracy involved in determining the velocity of propagation is large, the order of magnitude is still correct. Moreover, the results shown in table 1 are the average of a few sets of similar results. However, some of the velocities of propagation found have magnitudes greater than the speed of sound. This may again indicate that the propagation is at an angle to the axes but not normal to it.

Thus it has been established without doubt that a pressure field exists within the potential cone of the jet. The evidence of strong radial correlation within the potential cone and the evidence of velocity of propagation with the speed of sound indicate the presence of the pressure field in the cone.

3.5. *Longitudinal cross-correlation coefficient within the potential cone*

In the potential cone, the fluctuating components measured by the hot wire are small in comparison with the turbulence intensity of the wakes of the hot wire. Thus for the longitudinal cross-correlation measurement inside the potential cone which involves the moving wire situated immediately downstream of the other wire, the interference effect between the two wires can no longer be neglected (Ko & Davies 1971). This effect can be easily seen in figure 8(*b*), and the correlogram at a particular condition is shown in figure 8(*a*). The inverse relationship of the coefficient to the r.m.s. value of the turbulence intensity of the downstream signal can be easily seen.

By defining the longitudinal cross-correlation coefficient as

$$R_{x\tau} = \overline{u(x)\,u(x+\Delta x,\tau)}/\hat{u}(x)\,\hat{u}(x+\Delta x,\tau),$$

the cross correlogram obtained in the potential cone is shown in figure 8(*a*). It is quite different from the one in the mixing region, figure 9. Except that the value of the peak correlation coefficient differs, which is due to the inverse relationship mentioned above, the shape of every curve at different separation is very similar. This similarity suggests that the two hot wires inside the potential cone were sensing the same pressure field.

This pressure field can be further verified by the filtered longitudinal cross-correlation coefficients, figure 10, in which a centre frequency of 2 kHz with a $\frac{1}{3}$ octave bandwidth was used. Extremely good correlations exist for all the separations shown.

3.6. *Axial convection velocity in the potential cone*

The non-frozen nature of the turbulence structure within the mixing region convecting downstream is well known (Fisher & Davies 1964). It was shown by Davies, Fisher & Barratt (1963), and Bradshaw *et al.* (1964) that the convection velocity is higher than the local mean velocity in the outer half of the mixing region, but lower in the inner region. Also Fisher & Davies (1964) found that for

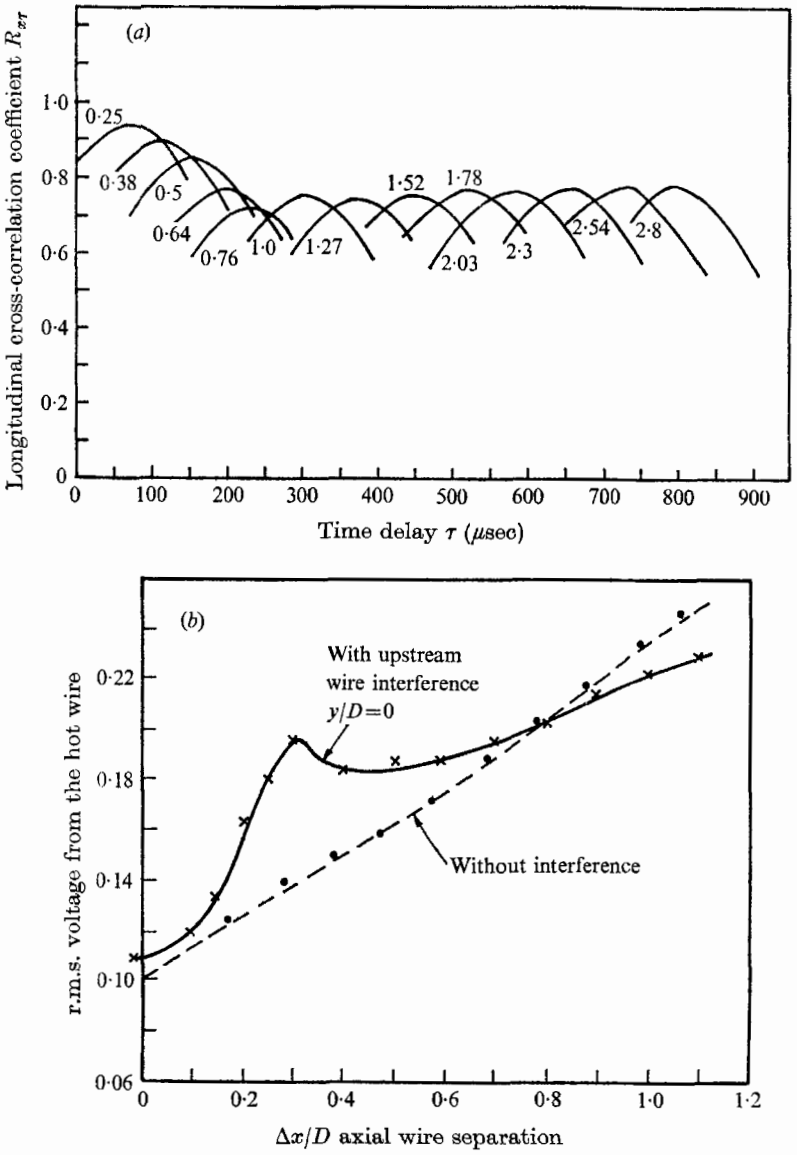

FIGURE 8. (*a*) Longitudinal cross-correlation coefficient against time delay for different wire separations (numbers on curves represent separation in cm). (*b*) Interference effect of the upstream wire on the downstream wire output. 2·5 cm diameter jet, $x/D = 1{\cdot}5$, $y/D = 0$, $\bar{U}_0 = 50$ m/sec.

a 2·5 cm diameter jet the convection velocity at a centre band filter of 2 kHz was the same as the overall convection velocity, a ratio of $\overline{U}_c/\overline{U}_0 = 0{\cdot}6$. This means that the dominant component of the turbulent field is due to the components around 2 kHz, which contribute the same overall and filtered convection velocity. Not surprisingly, the dominant components around 2 kHz observed above of the 2·5 cm diameter jet, are responsible for the pressure field found by the longitudinal cross-correlation coefficient curves, as shown in figure 10.

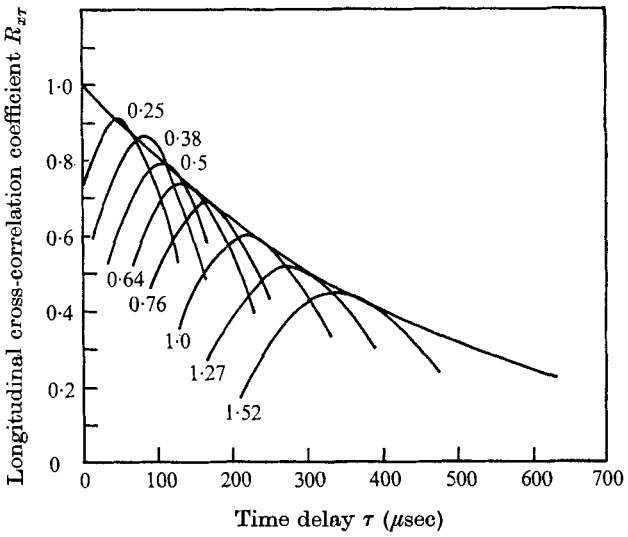

FIGURE 9. Longitudinal cross-correlation coefficient against time delay. Fixed wire delayed with respect to moving wire. 2·5 cm diameter jet; finite wire at $x/D = 1{\cdot}5$; $y/D = 0{\cdot}5$, $M_0 = 0{\cdot}22$. (Numbers on curves represent separation Δx cm.)

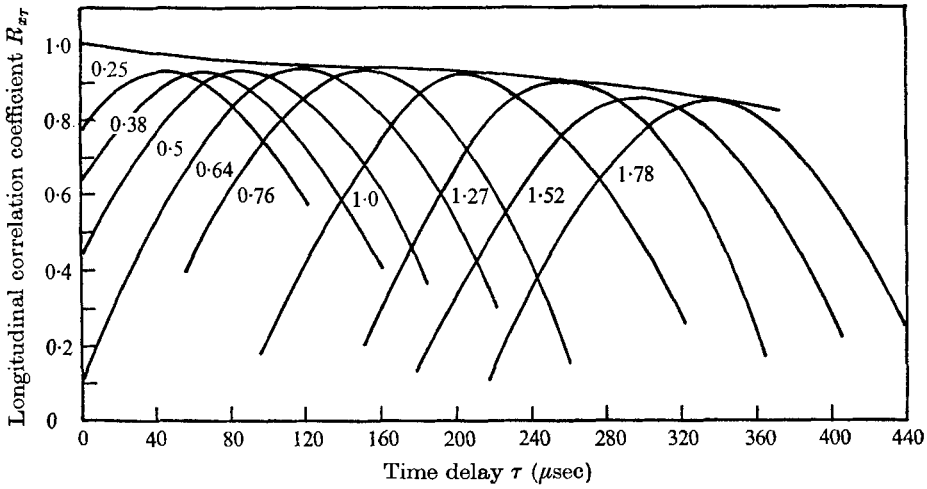

FIGURE 10. Longitudinal cross-correlation coefficient against time delay filtered in $\frac{1}{3}$ octave band. Centre band frequency = 2 kHz. 2·5 cm diameter jet; fixed wire at $x/D = 1{\cdot}5$; $y/D = 0{\cdot}1$, $M_0 = 0{\cdot}22$. Fixed wire delayed with respect to moving wire. (Numbers on curves represent separation Δx cm.)

The axial convection velocity within the potential cone is obtained from figures 8, 9 and 10 and other correlograms. It is plotted in figure 11. Although there is a bit of scatter, the radial distribution of the convection velocities within the potential cone is fairly constant at 0·65 $\overline{U}_0$ until the mixing region starts.

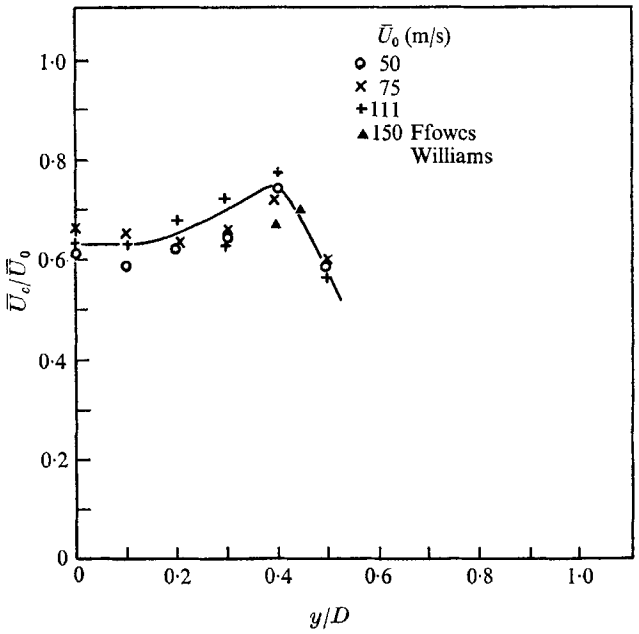

FIGURE 11. Radial distribution of convection velocity for different axial positions. x/D = 1·5, D = 2·5 cm.

The filtered convection velocity at the centre frequency of 2 kHz is constant at the axial position of x/D = 1·5, as shown in figure 12. It has a value of 0·65 $\overline{U}_0$, except in the source region (y/D = 0·5) where it is 0·6 $\overline{U}_0$. Similar constant values were found for x/D = 3. Unfortunately, there are not sufficient results from other workers for the evidence to be conclusive. But it seems that the pressure field in the potential cone propagates with a different convection velocity from the near field outside the jet, that is, 0·65 $\overline{U}_0$ instead of 0·72 $\overline{U}_0$ as found by Ffowcs Williams (1960).

It is suprising to find that the convection velocity of the near field in the potential cone is lower in value than that obtained in the near field outside the jet. This is because in the mixing (source) region the higher convection velocity occurs in the inner half of the region. Therefore, it would be expected that the higher speed eddies nearer to the potential cone would dominate the convection pattern of the field there and give a higher value than the pressure field outside which might be dominated by the closer and lower speed eddies. However, this difference in the convection velocity between the two pressure fields may be due to the motion of the medium in which the pressure field exists. But an investigation has to be done before a definite conclusion can be reached on this point.

Since the effect of the motion of the medium on the value of the convection velocity obtained in the potential cone is not known, it is difficult to predict whether the major contribution to the pressure field is due to the eddies which move at the same velocity or not. Assuming the motion of the medium has no effect on the convection velocity obtained, then the region where the eddies travel at $0{\cdot}65\,\overline{U}_0$ is in the high intensity region but nearer to the cone than the region of the maximum intensity.

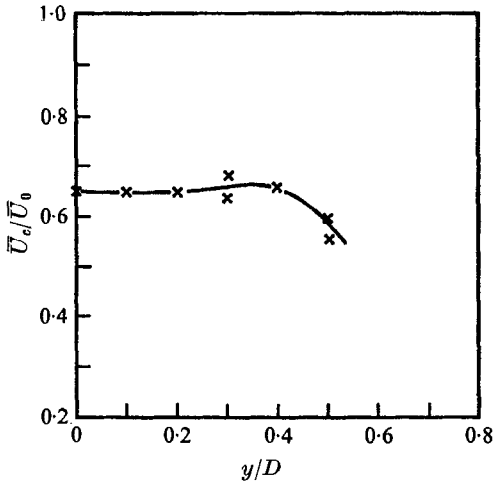

FIGURE 12. Radial distribution of convection velocity (filtered at the centre frequency of 2 kHz). $x/D = 1{\cdot}5$, $M_0 = 0{\cdot}22$, $D = 2{\cdot}5$ cm.

Similar to the results obtained in the mixing region, the overall convection velocity in the potential cone is the same for the filtered velocity at 2 kHz, figures 11 and 12. This confirms that in the 2·5 cm diameter jet the dominant components in the pressure field in the potential cone are around 2 kHz and are roughly the same dominant frequencies as in the mixing region. Thus, the field in the inner cone is due to the eddies generated in the mixing region.

Although the above argument concerning the relationship between the pressure field and the eddies by means of the axial convection velocity is not conclusive, the approach of comparing their respective convection velocities seems to offer a better understanding of them. Unfortunately, insufficient longitudinal cross-correlation coefficient measurements were made to yield the convection velocity in the potential cone and in the near field outside, for detailed comparison between the source region and the two associated near fields. Furthermore, the inaccuracy and the time involved in determining the velocity of convection may hinder further understanding of the eddies and the pressure fields.

3.7. *Longitudinal space correlation coefficient*

The longitudinal space correlograms in the near field outside the jet show a very lightly damped cosine curve as the spatial distance increases (Franklin & Foxwell 1958). From the inverse relationship between the spectrum and the longitudinal space correlogram, the lightly damped cosine characteristics are

due to the presence of dominant components of noise. Since the pressure field inside the potential cone is also under the influence of the same sources, one would expect similar correlograms as the ones outside the jet. This is the case shown in figure 13. Further, as in the case of the near field outside, the coefficient curves found in the potential cone are independent of exit velocity.

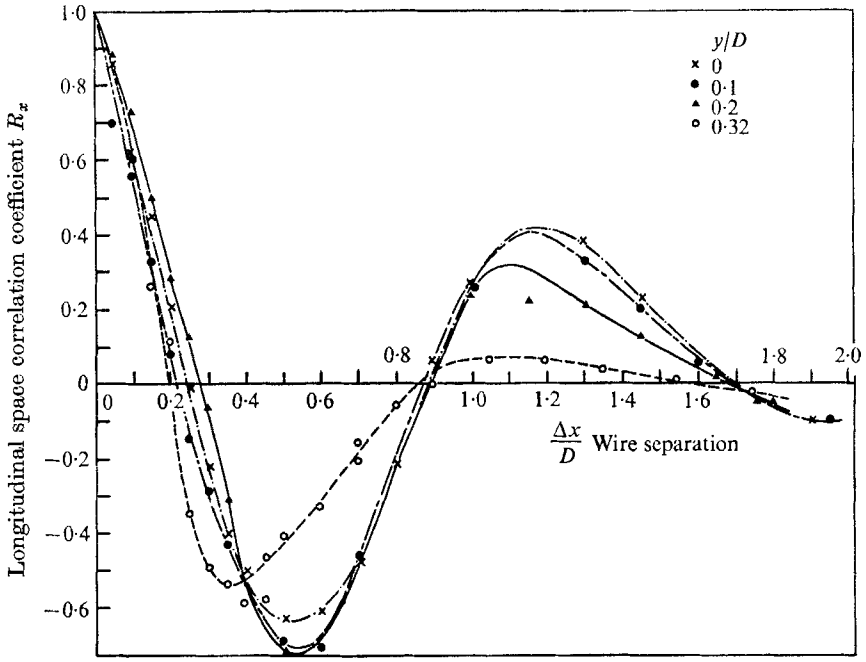

FIGURE 13. Radial distribution of longitudinal space correlation against axial wire separation. $x/D = 1{\cdot}5$, $M_0 = 0{\cdot}218$, $D = 5$ cm.

3.8. *Spectrum inside the potential cone*

As has been shown by Lassiter & Hubbard (1956), the spectrum of the near field outside the jet shows a broad peak with most of the energy around the peak. It is well known that in the mixing region of the jet, the spectrum covers an appreciable range of frequency and is continuous (Davies *et al.* 1963). However, the ones in the potential cone would show characteristics similar to the ones in the near field outside.

Figure 14(*a*) shows the spectra of the 5 cm diameter jets for different axial distance downstream from the nozzle. The results are all obtained at the jet axes, $y/D = 0$, $z/D = 0$ and at a constant exit Mach number of 0·218. One spectrum at $x/D = -0{\cdot}25$, that is, inside the nozzle, is also shown. It can be seen that for the spectrum at $x/D = -0{\cdot}25$, besides the hum at 50 Hz, the spectrum decreases more or less in a straight line at approximately 3·5 dB/octave with increase in frequency. A similar trend is also shown by the spectra at the axial positions of $x/D = 0$ and 0·25. In actual fact, they overlap each other to form a single curve. This complete absence of any peak except for the 50 Hz hum, within the first quarter diameter downstream of the nozzle exit, indicates that

no near field pressure is present in the signal and the nozzle is more or less free from the noise generated by the control valve.

From a distance of half a diameter downstream, the spectrum shows the trace of a small 'bump' around the frequency of 600 to 1000 Hz. This 'bump' consists of the extra energy sensed by the hot wire either due to the presence of hydrodynamic pressure associated with the eddies or due to the increase in

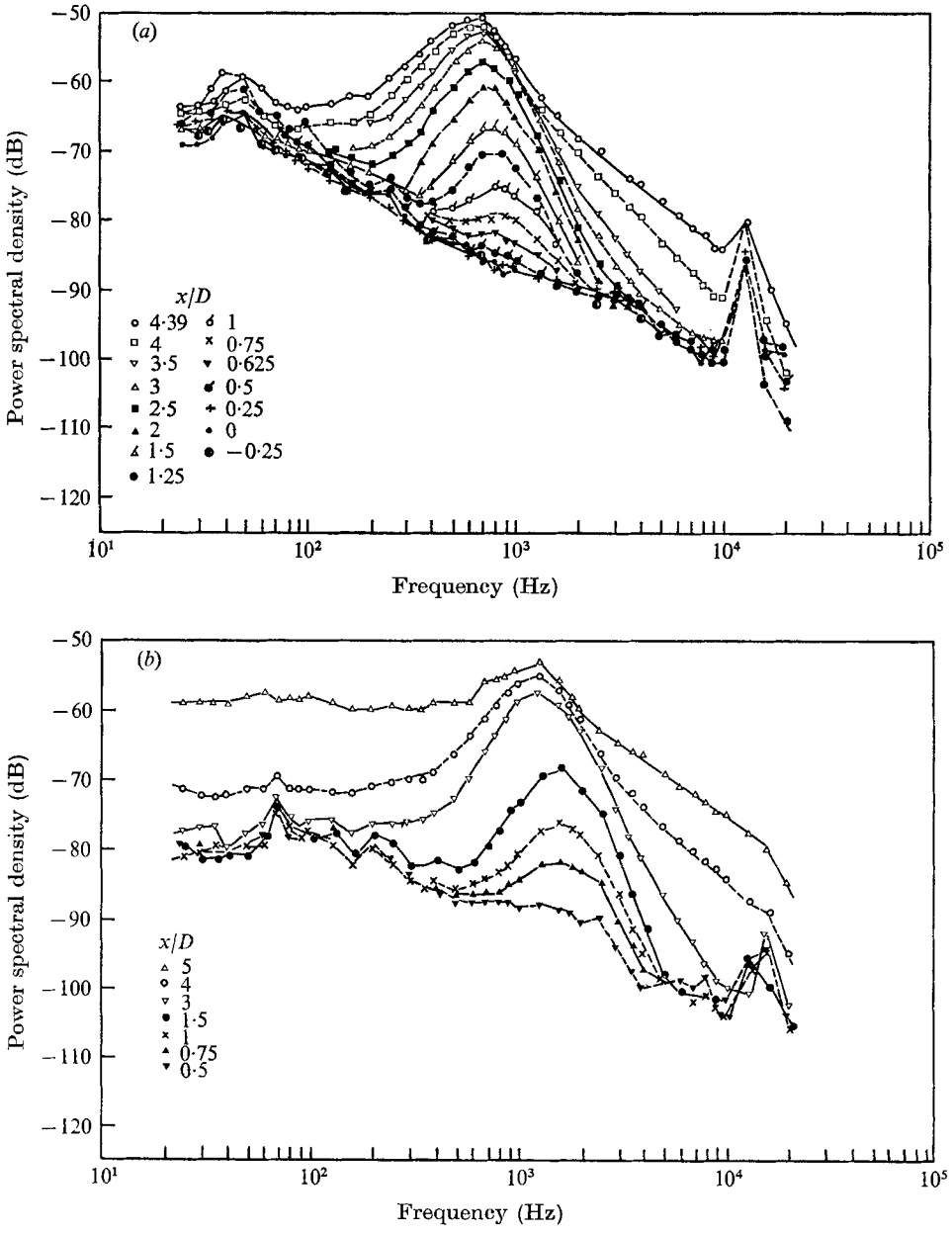

FIGURE 14. Power spectra for different axial positions. (*a*) 5 cm diameter jet, $M_0 = 0{\cdot}218$, $y/D = 0$. (*b*) 2·5 cm diameter jet, $M_0 = 0{\cdot}22$, $y/D = 0$.

the local turbulence intensity, or to both effects. A separation between these causes is impossible without further evidence. Furthermore, besides this increase in energy, the frequency bandwidth under the 'bump' increases as the measuring point is moved further downstream.

Between the axial position of $x/D = 2$ to 3 the difference in the spectral level between the peak and the trough is as high as 15 dB. The slope on the low frequency sides can be as high as 15 dB/octave and the one on the high frequency side 20 dB/octave.

As the axial distance, x/D, increases, the spectral level at low frequency increases and so does that at high frequency. But it seems that they do not begin to change until $x/D = 1{\cdot}5$ or 2 for the low frequency side and $x/D = 2{\cdot}5$ for the high frequency side above 3·5 kHz. This suggests that the increase in energy between the nozzle and 2 diameters downstream is more or less wholly absorbed in building up the 'bump' to its optimum condition and shape. This may also suggest that most of the energy increase is due to the increase in the pressure field at the dominant frequencies and very little is due to increase in the local turbulence.

The spectrum shape is completely different from that in the mixing region. The frequency of the peak in the spectrum occurs in the range 600 to 800 Hz for the 5 cm diameter jet and this frequency shifts from roughly 800 Hz for $x/D = 0{\cdot}5$ to 650 Hz for $x/D = 4{\cdot}39$. This decrease in the peak frequency with respect to the increase in the axial distance has the same trend as the near-field results outside the jet (figure 18).

The increase in the bandwidth of the 'bump' as the axial distance increases can be explained by the directivity effect of the hydrodynamic field, since the field will propagate more in the downstream than the upstream direction. Therefore, at a position further downstream, the hot wire will not only sense the local pressure field but also that from sources further upstream.

The spectra of the 2·5 cm diameter jet are similar to the 5 cm ones and are shown in figure 14(*b*). The frequency of the peak varies between 1·3 to 1·6 kHz. This diameter dependence will be shown in the section on the Strouhal number. Further from figure 14(*b*), the spectrum at $x/D = 5$ shows that although the low frequency spectral level increases by 13 dB, the energy level of the peak increases only by 2 dB. This, then, explains the reason why in the mixing region, for example, at the maximum shear region, such a 'bump' could not be found. It is because the high background turbulence energy level completely obscures the comparatively small pressure fluctuations. Thus, this indicates that the flat part of the spectrum is due to the local turbulence, while the peak represents mostly the pressure field.

Comparison between the spectra in the near field outside (figure 23) and in the potential cone (figure 14) shows the absence of the flat and constant spectral level at the low frequency side for the spectra outside. The other difference is the slope at the high frequency side of the peak. Without the influence of the local turbulence the spectra of the near field outside have a constant slope for $x/D = 0{\cdot}5$ to 4·5 (figure 23). However, in the potential cone, constant slope is maintained only between $x/D = 1$ to 3, where the local turbulence is small.

Beyond the axial distance of $x/D = 3$ the effect of the local turbulence reduces the slope and a value of 6 dB/octave is obtained at $x/D = 5$. This 6 dB/octave slope is the same as that obtained within the mixing region (figure 16). Without the influence of local turbulence, further comparison yields that the rate of decrease in the high frequency side of the spectra in the two fields is the same. A value for this rate of decrease is about 19 dB/octave. Thus, from the variation of the rate of decrease, it suggests that the slope is also a very good indication of the influence or presence of the pressure field. Any value between the

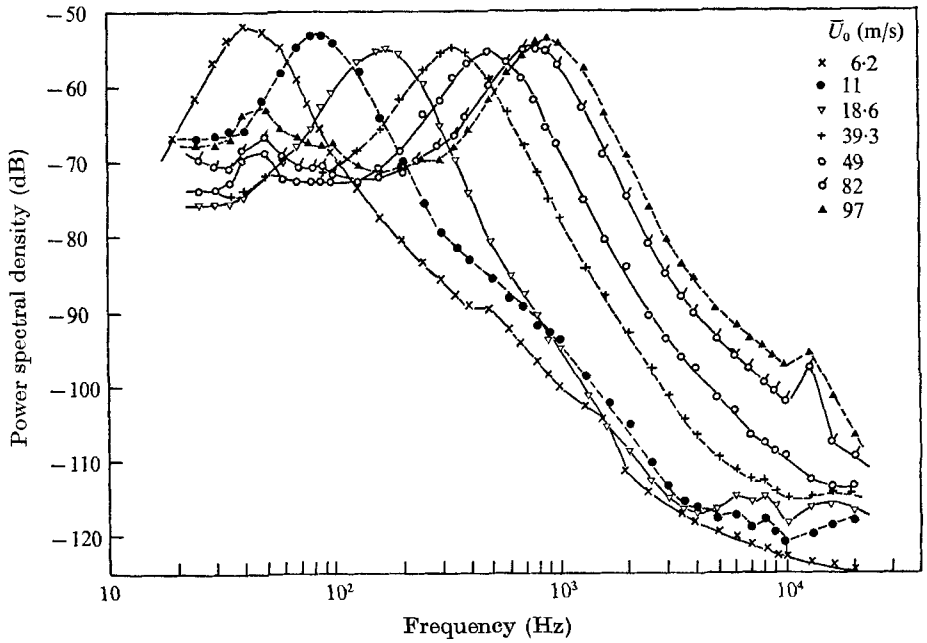

FIGURE 15. Power spectrum against jet exit speed. 5 cm diameter jet, $x/D = 3$, $y/D = 0$.

6 dB/octave for turbulence and 19 dB/octave for pressure indicates the combined effect of both of them.

The variation of spectrum shape with jet exit velocity is shown on figure 15. With other results, not shown here, the shape of the pressure spectrum is found to be the same, irrespective of axial position, jet velocity and jet diameter.

Typical spectra at different radial positions, y/D, are shown in figure 16. The masking of the pressure spectrum by the turbulence spectrum can be easily seen, as the mixing region is approached.

3.9. *Strouhal number inside the potential cone*

The peak frequency observed above can be expressed in terms of the Strouhal number, $f_p D/\bar{U}_0$, where f_p, D and $\bar{U}_0$ are the peak frequency, jet diameter and exit velocity. Figures 17 (*a*) and (*b*) show the typical relationship between the Strouhal number and the Mach number at $x/D = 1{\cdot}5$ and 4; $y/D = 0$. Results

from both jets are plotted. The same slope is attained for all the axial positions along the axis, $0{\cdot}75 \leqslant x/D \leqslant 4$, in the Mach number range $0{\cdot}06 \leqslant M_0 \leqslant 0{\cdot}4$. Results of the peak Strouhal number obtained outside the jet ($y/D = 1{\cdot}0$) are also shown.

Within the Mach number range shown, the value of the Strouhal number for the near field inside the potential cone is higher than the corresponding value outside the jet. This difference increases as the Mach number increases.

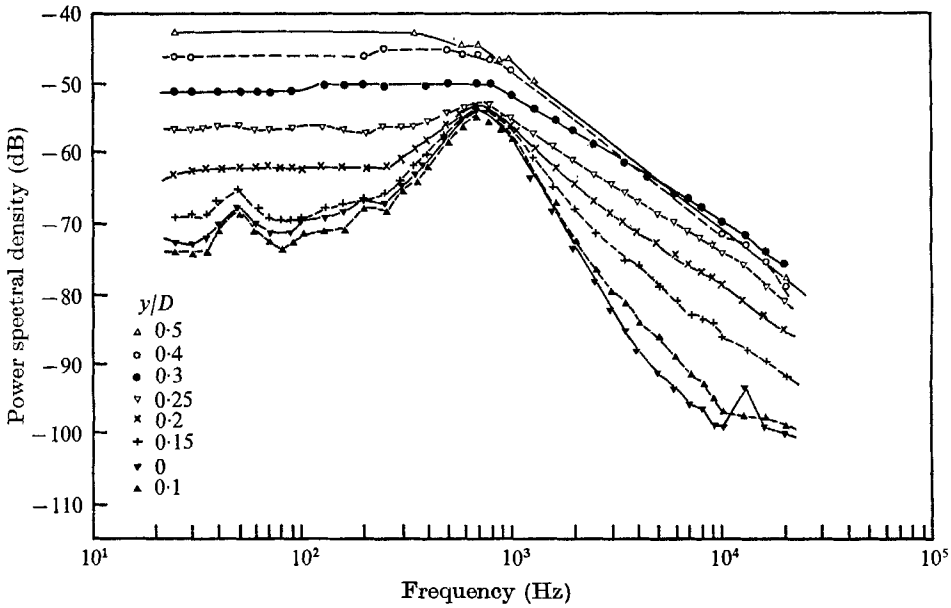

FIGURE 16. Power spectrum for different radial positions. 5 cm diameter jet, $x/D = 3$, $M_0 = 0{\cdot}218$.

At a Mach number of 0·218, a comparison of the Strouhal numbers of the two fields with the axial distance is shown in figure 18. The rate of decrease of the Strouhal number with the axial distance is approximately the same for the two cases. At an exit velocity of $M_0 = 0{\cdot}218$, the peak Strouhal numbers in the potential cone, along the outer jet boundary ($\theta = 10°$) and in the mixing region ($y/D = 0{\cdot}5$), are shown in figure 19. There are frequency shifts between the potential cone, mixing region and the near field outside the jet. For $x/D > 1$, the Strouhal number in the potential cone is higher than the ones obtained in the mixing region. Further, the one in the mixing region is higher than the one in the near field outside the jet.

The radial distribution of the Strouhal number is shown in figures 20(*a*) and (*b*) for $x/D = 0{\cdot}75$ and 1·5. Results obtained further downstream up to $x/D = 4$ are similar to figure 20(*b*). Although there is some scatter in figure 20(*a*), the peak frequency or Strouhal number attains its maximum at $y/D = 0{\cdot}4$. Limited results from Laurence (1956) are also shown in figure 20(*a*). At $x/D = 1{\cdot}5$ (figure 20(*b*)) the sharp peak is replaced by a low peak. Results of Bradshaw *et al.* (1964) agree

with the results shown in figure 20(*b*). At $x/D = 3$, the same peak occurs at $y/D = 0{\cdot}15$ but the peak disappears completely by $x/D = 4$.

By marking the position of the maximum Strouhal number in the radial

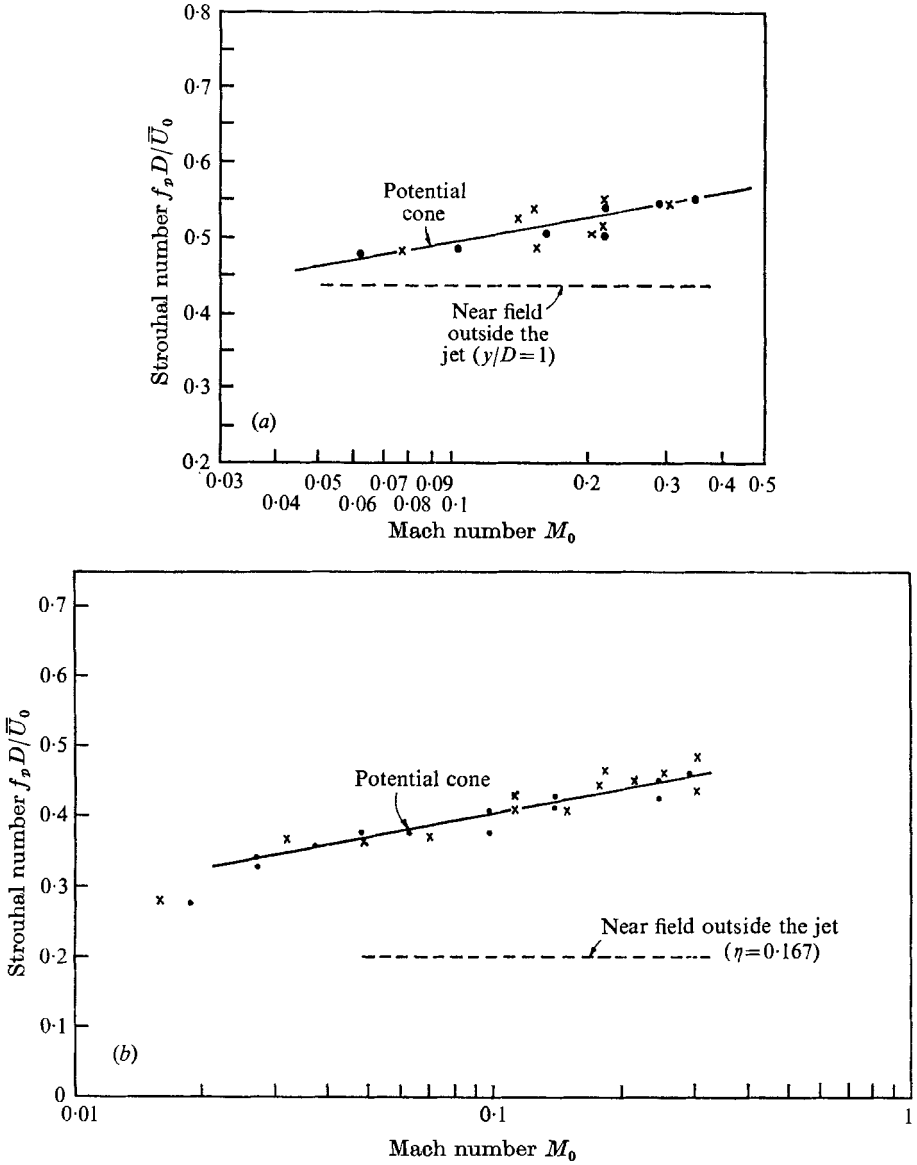

FIGURE 17. Strouhal number against Mach number for different jets and axial positions inside the potential cone. (*a*) $x/D = 1{\cdot}5$, $y/D = 0$. (*b*) $x/D = 4$, $y/D = 0$. ×, $D = 5$ cm; ●, $D = 2{\cdot}5$ cm.

direction for the different axial positions in figure 7, it is interesting to find that they all lie on the boundary of the potential cone with the mixing region. Surprisingly, for the near field outside the jet, as will be shown later, the peak frequencies of the spectra are found along the outer boundary of the jet ($\theta = 10°$).

Further, similar to the field in the potential cone, there is no maximum in the radial distribution of the Strouhal number outside the jet beyond $x/D = 4$. This suggests similar characteristics of the two pressure fields.

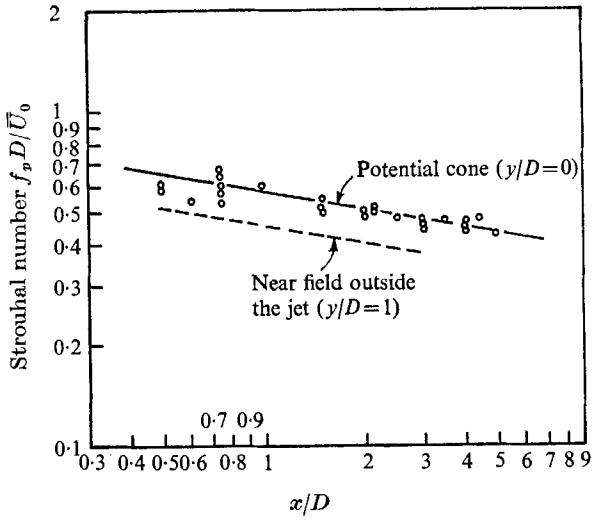

FIGURE 18. Comparison of the Strouhal number against axial distance of the two near fields inside the potential cone and outside the jet. $M_0 = 0{\cdot}218$, 2·5 and 5 cm diameter jets.

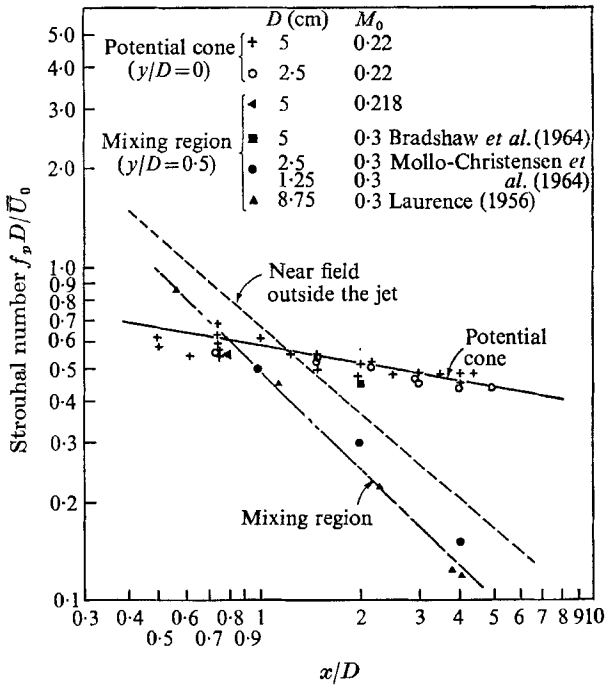

FIGURE 19. Strouhal number against axial distance inside the potential cone. $y/D = 0$, $M_0 = 0{\cdot}22$.

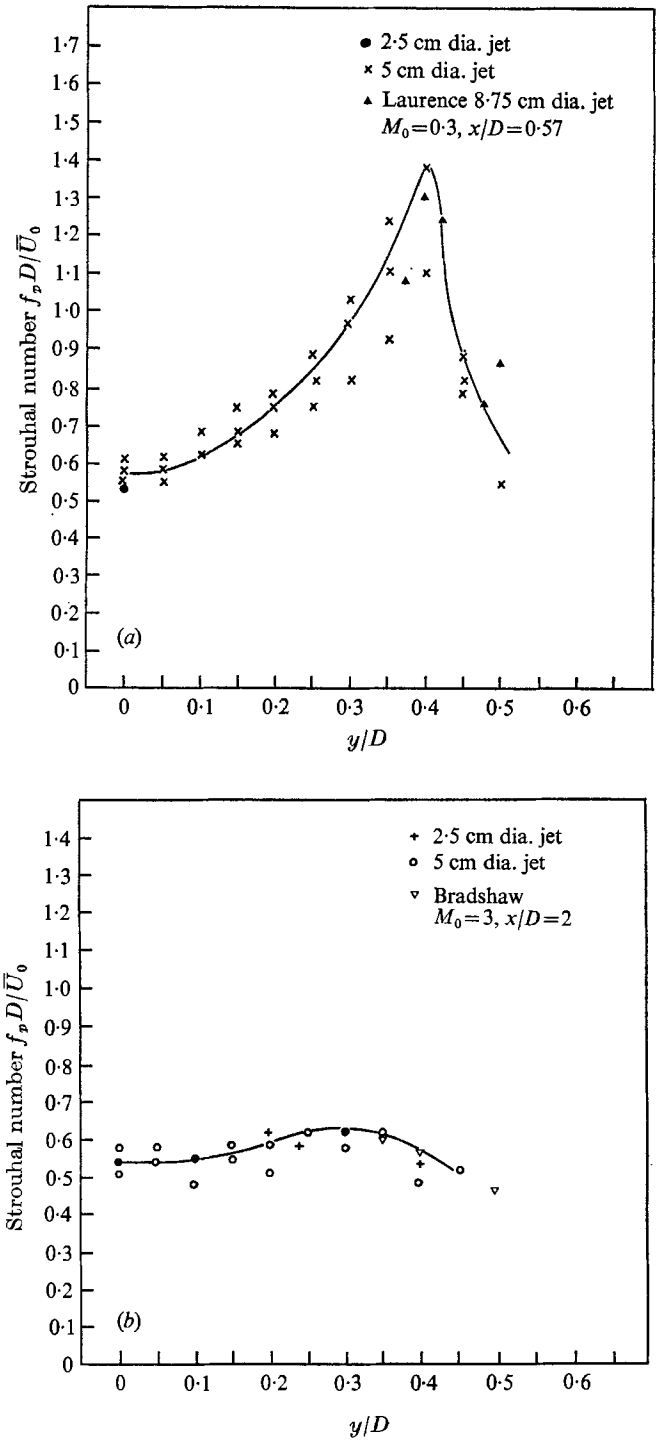

FIGURE 20. Strouhal number against radial distance. (*a*) x/D = 0·75, M_0 = 0·218. (*b*) x/D = 1·5, M_0 = 0·218.

The greater rate of increase in the Strouhal number to the maximum value for the axial position nearer to the axis (figure 20(*a*)) say, at $x/D = 0{\cdot}75$, may be due to the Doppler effect of the moving source.

The other reason for the different rate of increase may be the effect due to the directivity. Because of this effect the instrument measurements obtained very near the nozzle exit are due to the immediate sources. Further downstream the instrument measured not only the pressure fluctuations from the immediate sources, but also the ones generated by the upstream sources.

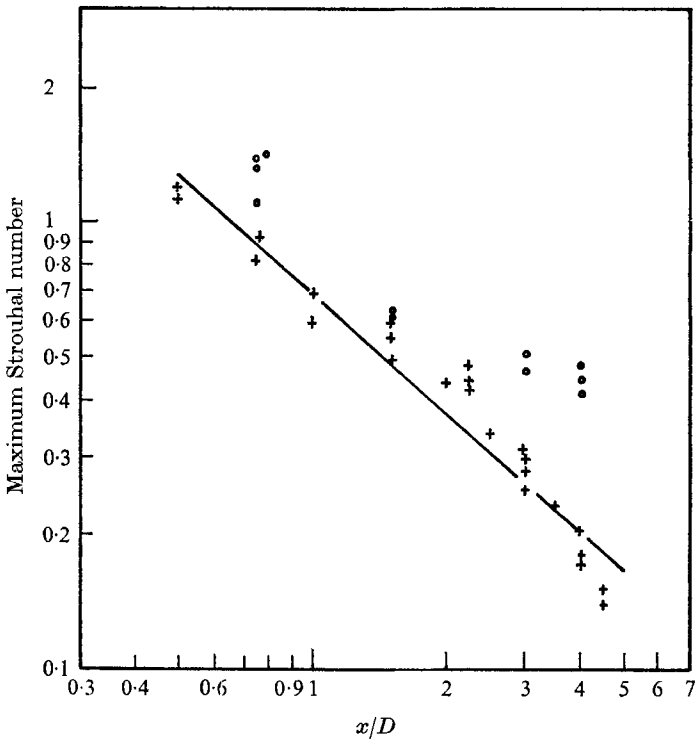

FIGURE 21. Comparison of the maximum Strouhal number of the two near fields inside the potential cone and outside the jet. $M_0 = 0{\cdot}218$, 2·5 and 5 cm diameter jets. ○, potential cone ($\theta = -6°$); +, near field outside the jet ($\theta = 10°$).

A comparison of the maximum Strouhal number for different radial distributions in the two near fields is shown in figure 21. As has been mentioned previously, the maximum Strouhal number of the two fields lies on the inner and outer boundaries of the jet.

3.10. *Near field outside the jet*

Although pressure measurements in the near field outside the jet have been made by a number of workers, detailed results were not available for comparison with the field inside the potential cone. Although the jet was not situated within an anechoic chamber, the reflected pressure field should be small within the zone of investigation, which was radially one diameter away from the jet boundary. Thus, no allowance was made for reverberation.

In the near field outside, the slope of the overall pressure to jet exit velocity may vary between 3 and 8, depending upon the radial position (Lassiter & Hubbard 1956, Howes *et al.* 1957, and others). However, the above case is true only when the exit velocity is higher than 40 m/sec as shown in figure 22. This means that the hydrodynamic pressure associated with the vortices is quite different from the one of eddies.

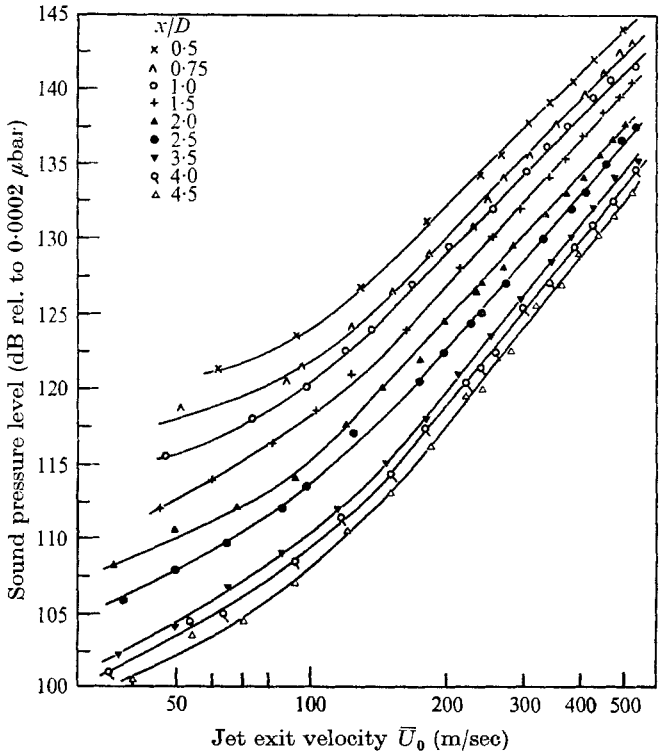

FIGURE 22. Effect of jet exit velocity on overall sound pressure level in the near field outside the jet. 5 cm diameter jet, $\eta = 0{\cdot}167$ ($\theta = 10°$), $\frac{1}{4}$ in. microphone.

3.11. *Noise spectrum outside the jet*

At the jet boundary, $\theta = 10°$, the axial variation of the spectrum is shown in figure 23 where each spectrum possesses a single broad peak. The peak frequency is a function of the axial distance. This shows that the higher frequency noise comes from the region very near the exit and the lower frequency noise from further downstream. In the spectrum the components above 10 kHz are due to the noise generated by the main control valve.

As has been shown by Howes *et al.* (1957) and Mollo-Christensen, Kolpin & Martuccelli (1964) similarity of the spectrum could be obtained by plotting the power spectral density, $F(f)$, against the Strouhal number, $fD/\bar{U}_0$, that is

$$F(f)/\{\rho_0 a_0^2 D G_2(\theta)\,(r/D)^{\alpha_1}\,(M)^{\alpha_2} G_3(Re_D)\} \propto (fD/\bar{U})^{\alpha_3}.$$

For the spectrum obtained at a particular position,

$$F(f)/\{D \times G_3(Re_D) \times M^{\alpha_2}\} \propto (fD/\bar{U})^{\alpha_3}.$$

From the results shown in figure 24(*a*) and (*b*) better similarity is obtained by considering $D \times G_3(Re_D)$ independent of the Strouhal number. Further, the corresponding α_2 were obtained from figure 22.

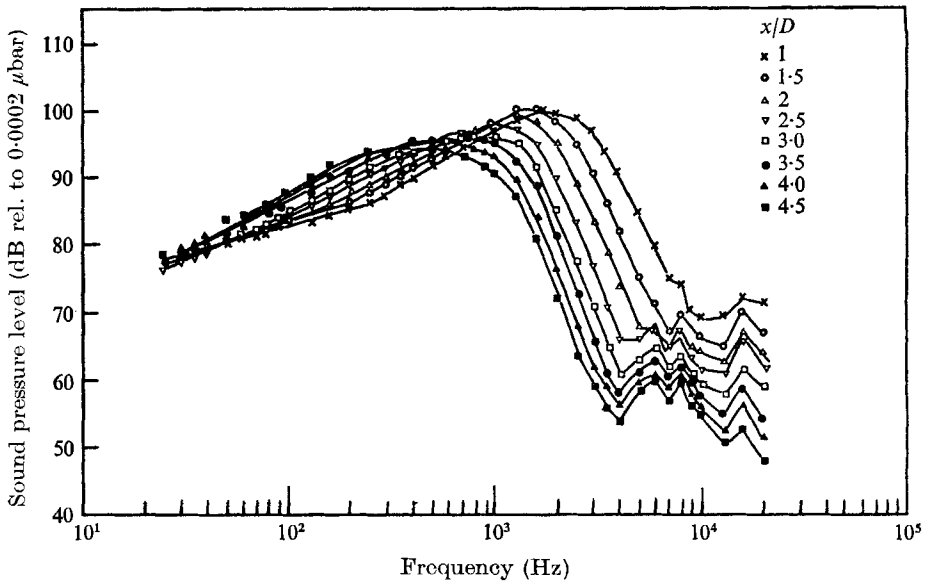

FIGURE 23. Axial distribution of the near field noise spectrum outside the jet. 2·5 cm diameter jet, $\theta = 10°$, $M_0 = 0{\cdot}22$, $\frac{1}{4}$ in. microphone.

Very good similarity is shown by the two figures over the velocity range of $\overline{U}_0 = 40$ to 140 m/sec. Only very slight deviation from the similarity curve is shown for velocity below 40 m/sec. The lower the velocity, the greater is the deviation. The reason for this deviation at the low velocity region is due to the difference in the behaviour of the vortex pressure fluctuations from those due to eddies. As shown in figure 22, no slope, α_2, can be obtained in the low velocity range, below 40 m/sec. Further comparison of the similarity curves at different axial positions shows the deviation is smaller when the spectra are obtained nearer to the nozzle exit than those from further downstream, figure 24(*a*) and (*b*).

3.12. *Strouhal number*

Similar to § 3.9, the peak frequency of the spectrum in the field outside can be represented by the Strouhal number. The Strouhal numbers obtained along the jet boundary ($\theta = 10°$) are shown in figure 25. The available results of other workers are also shown. Although there is quite a bit of scatter in the results of other workers, a straight line can be drawn with the results obtained in the present investigation (figure 25). The results from Hubbard & Lassiter (1953) agree very well with the new measurements, although their exit velocity was higher. Thus, there is agreement with other workers that the higher frequency noise is generated near the orifice while the lower frequency noise originates from further downstream.

The radial distribution of the Strouhal number for different axial positions is shown in figure 26. It shows that the rate of decrease of the Strouhal number very near to the jet is much higher than it is further away until a more or less constant value is reached.

The variation of the Strouhal number with the exit Mach number is shown in figure 27. Except at the axial position very near the orifice, $x/D \leqslant 0{\cdot}5$, the

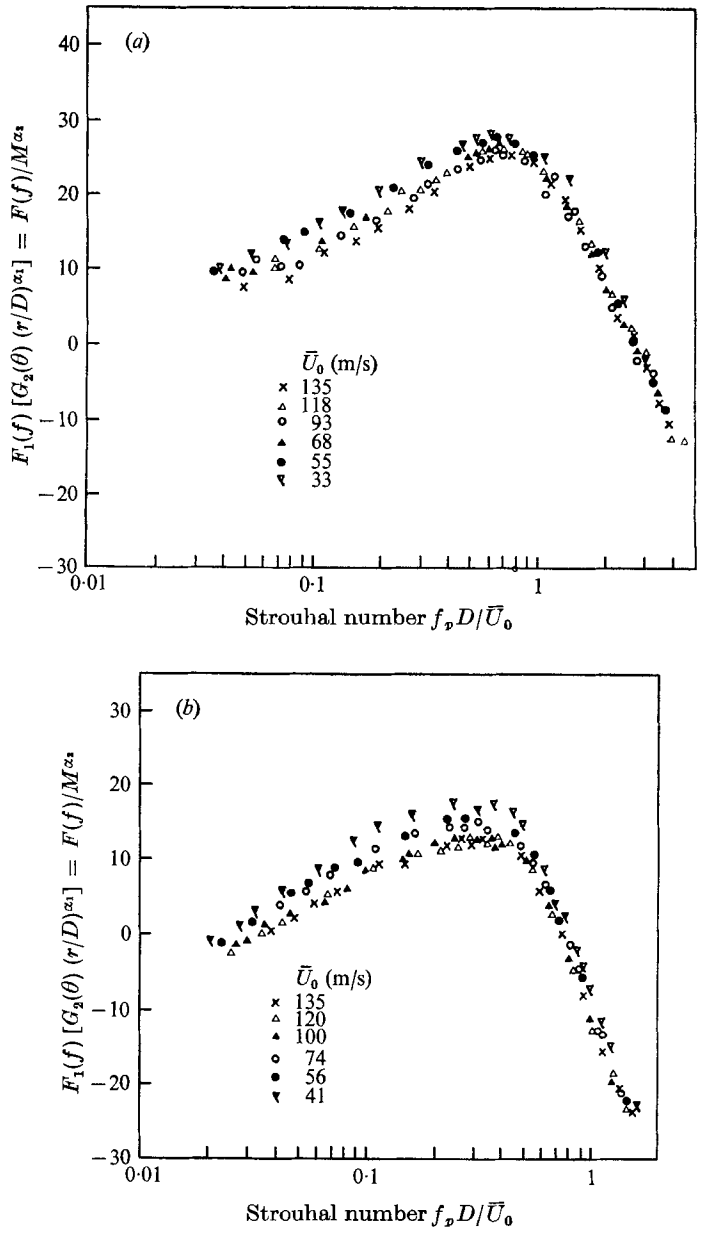

FIGURE 24. Similarity in sound pressure spectra in the near field outside the jet. 5 cm diameter jet, $\eta = 0{\cdot}167$, $\frac{1}{4}$ in. microphone. (*a*) $x/D = 1$, $\alpha_2 = 3{\cdot}14$. (*b*) $x/D = 3$, $\alpha_2 = 3{\cdot}52$.

Strouhal number is independent of the exit Mach number. This is different from the ones obtained in the potential cone. Thus, from the microphone measurements the vortex noise can still be distinguished from the eddy-generated noise. This vortex noise exists below an exit velocity of about 40 m/sec.

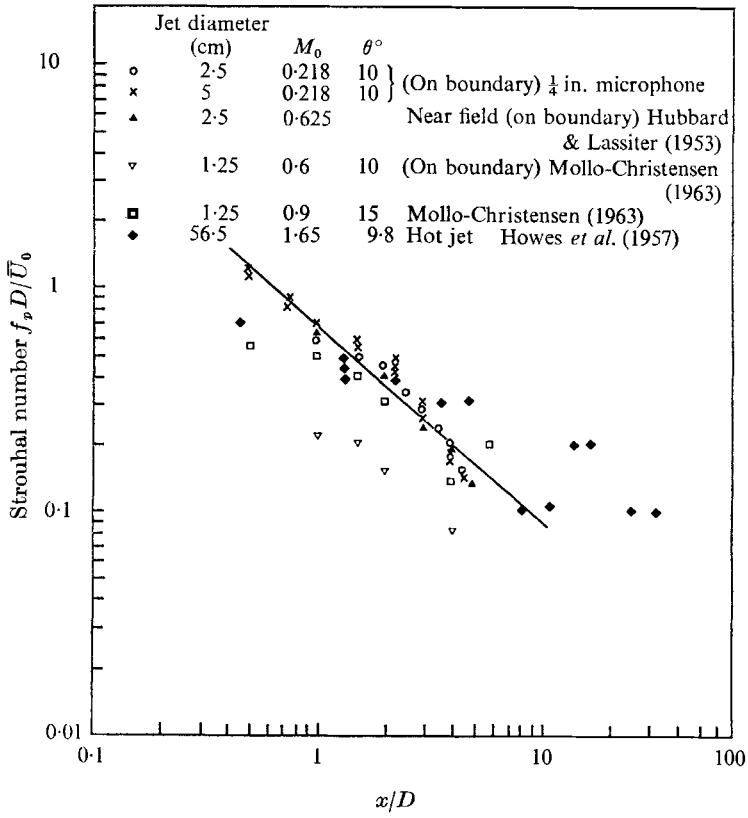

FIGURE 25. Axial distribution of Strouhal number in the near field outside the jet.

4. Conclusions

The hot-wire measurements in the potential cone of the jet have shown that a near field exists within the cone, except the first half diameter downstream. There are distinct differences between the pressure fluctuations generated by the vortices at low velocity and the fluctuations from eddies at higher velocity.

The radial axial cross-correlation and the space-correlation results of the pressure field within the potential cone show extremely good correlation.

The spectrum measured inside the cone has a high peak similar to the ones outside. The flat portion at low frequency indicates the effect of the local turbulent fluctuations.

The peak frequency of the spectrum obtained inside the cone, in terms of the Strouhal number, is found to be a function of the axial and radial positions and the exit velocity. This variation in the Strouhal number may indicate the Doppler

effect of moving source, moving medium and refraction of the sound waves in the noise producing region.

The detailed pressure measurements obtained in the near field outside tend

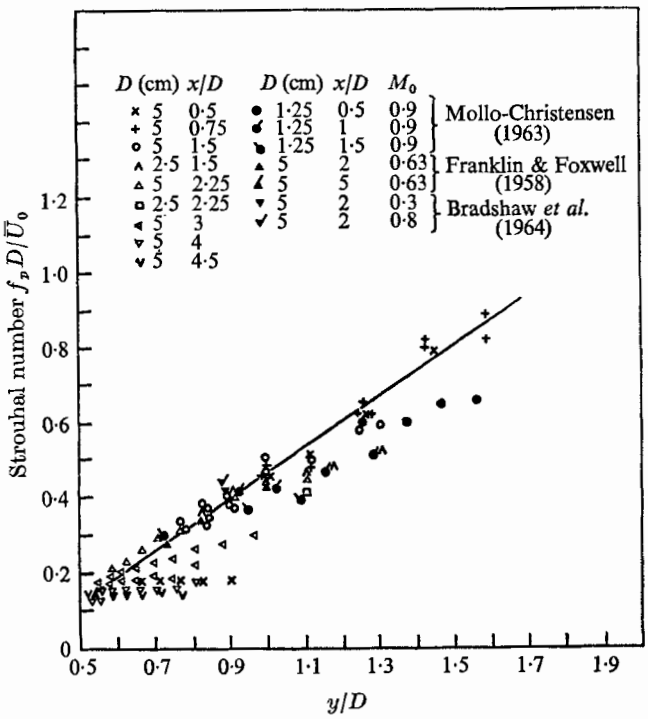

FIGURE 26. Radial distribution of the Strouhal number of the sound pressure spectra in the near field outside the jet. $M_0 = 0{\cdot}218$, $\frac{1}{4}$ in. microphone.

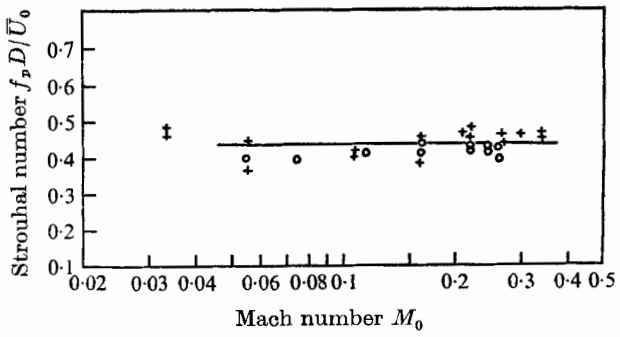

FIGURE 27. Strouhal number against Mach number in the near field outside the jet $x/D = 1{\cdot}5$, $\eta = 0{\cdot}333$, $y/D = 1$, $\frac{1}{4}$ in. microphone. +, $D = 5$ cm; ○, $D = 2{\cdot}5$ cm.

to agree with the results of other workers. Comparison of the corresponding Strouhal numbers in the two fields shows a frequency shift. A higher Strouhal number is obtained in the near field inside. This may be due to the effects of Doppler, refraction, motion of the medium and the presence of mean shear.

The authors wish to thank Professor E. J. Richards and other members of the department for the suggestions. Thanks are also due to the Ministry of Aviation for their interest and financial support.

REFERENCES

ALLCOCK, G. A., TANNER, P. L. & MCLACHLAN, K. R. 1962 A general purpose analogue correlator for the analysis of random noise signals. *University of Southampton. Aero. Astr. Rep.* 205.

BOSE, B. 1968 Experimental study of the wave-like characteristics of turbulence in shear layers and behind grids. Ph.D. thesis, University of Southampton.

BRADSHAW, P., FERRISS, D. H. & JOHNSON, R. F. 1964 Turbulence in the noise-producing region of a circular jet. *J. Fluid Mech.* **19**, 591–624.

DAVIES, P. O. A. L. & FISHER, M. J. 1964 Heat transfer from electrically-heated cylinders *Proc. Roy. Soc.* A **280**, 486–527.

DAVIES, P. O. A. L., FISHER, M. J. & BARRATT, M. J. 1963 The characteristics of the turbulence in the mixing region of a round jet. *J. Fluid Mech.* **15**, 337–367.

DAVIES, P. O. A. L. & KO, N. W. M. 1965 The near field generated by intense turbulence. *5th Int. Congress Acoustics*, Leige, paper L 53.

DAVIES, P. O. A. L., KO, N. W. M. & BOSE, B. 1967 The local pressure field of turbulent jets. *Aero. Res. Counc. Lond.* 29065. N. 518. Also 1968 *Aero. Res. Counc. Current Paper*, no. 989.

FFOWCS WILLIAMS, J. E. 1960 On convected turbulence and its relation to near field pressure. *University of Southampton, U.S.A.A. Rep.* 109.

FISHER, M. J. & DAVIES, P. O. A. L. 1964 Correlation measurements in a non-frozen pattern of turbulence. *J. Fluid Mech.* **18**, 97–116.

FRANKLIN, R. E. & FOXWELL, F. H. 1958 Correlation in the random pressure field close to a jet. *Aero. Res. Counc. Lond. R & M* 3161.

HOWES, W. L., CALLAGHAN, E. E., COLES, W. D. & MULL, H. R. 1957 Near noise field of a jet engine exhaust. *N.A.C.A. Rep* 1338.

HUBBARD, H. H. & LASSITER, L. W. 1953 Experimental studies of jet noise. *J. Acous. Soc. Am.* **25**, 381–384.

KO, N. W. M. 1969 The near field structure of subsonic cold jets. Ph.D. thesis. University of Southampton.

KO, N. W. M. & DAVIES, P. O. A. L. 1971 Interference effect of hot wires. *IEEE Transactions on Instrumentation and Measurement.* IM–20 (1), 76–78.

LASSITER, L. W. & HUBBARD, H. H. 1956 The near noise field of static jets and some model studies of devices for noise reduction. *N.A.C.A. Rep.* 1261.

LAURENCE, J. C. 1956 Intensity, scale and spectra of turbulence in the mixing region of a free subsonic jet. *N.A.C.A. Rep.* 1292.

MOLLO-CHRISTENSEN, E. 1963 Measurement of near field pressure of subsonic jets. *A.G.A.R.D. Rep.* 449.

MOLLO-CHRISTENSEN, E., KOLPIN, M. A. & MARTUCCELLI, J. R. 1964 Experiments on jet flows and jet noise for field spectra and directivity patterns. *J. Fluid Mech.* **18**, 285–301.